VTT Technical Research Centre of Finland

Cascaded superconducting junction refrigerators

Kemppinen, Antti; Ronzani, Alberto; Mykkänen, Emma; Hätinen, Joel; Lehtinen, Janne S.; Prunnila, Mika

Link to publication

Cascaded superconducting junction refrigerators: optimization and performance limits

A. Kemppinen,* A. Ronzani, E. Mykkänen, J. Hätinen, J. S. Lehtinen, and M. Prunnila

VTT Technical Research Centre of Finland Ltd

(Dated: September 30, 2020)

We demonstrate highly transparent vanadium–silicon and aluminium–silicon tunnel junctions, where silicon is doped to remain conducting even in cryogenic temperatures. We discuss using them in a cascaded electronic refrigerator with two or more refrigeration stages, and where different superconducting gaps are needed for different temperatures. The optimization of the whole cascade is a multidimensional problem, but we present an approximative optimization criterion that can be used as a figure of merit for a single stage only.

Normal metal – insulator – superconductor (NIS) and semiconductor – superconductor (Sm–S) tunnel junctions can be used for electrical refrigeration, since the superconducting energy gap Δ allows thermionic energy filtering of the tunneling electrons [1–4]. Remarkable proof-of-concept demonstrations using suspended lateral assemblies with cold fingers include the refrigeration of macroscopic objects [5–7], but despite the extensive efforts, miniature electrical refrigerators have not been able to replace more macroscopic techniques such as dilution refrigeration. Challenges for practical applications include limited cooling power and complicated engineering of phonon and electron-phonon heat flows in cold finger solutions [8, 9], and the limited temperature range for refrigeration that depends on Δ. The latter could in principle be overcome by multi-stage refrigerators that utilize superconductors with different Δ [10–12], but still, practical multi-stage refrigerators have not been demonstrated.

Recently, the electronic refrigeration of a macroscopic silicon chip was demonstrated using aluminium–silicon junctions as the electronic cooling element, mechanical support, and as a blockade for phonon heat transport [13]. Phonon transport was suppressed simply by the Kapitza resistance between Al and Si [14]. This approach avoids complex arrangements of cold fingers, which should allow a simple multi-stage assembly, possibly even 3D integration, see Fig. 1(a). Reference [13] concludes that refrigeration from above 1 K to below 100 mK is a realistic target, but improvements are still needed: *(i)* Since both cooling power and phonon heat leaks are proportional to the tunnel junction area A, it is beneficial to decrease the characteristic resistance $R_A = R_T A$ to improve the ratio between cooling power and phonon heat leaks. Here, R_T is the tunneling resistance of the junction. *(ii)* While the Kapitza interface appeared to be a sufficient heat block below about 500 mK, the suppression of phonon heat conductance using, e.g., nanowire constrictions, is necessary at higher temperatures. *(iii)* A superconductor with larger gap than aluminium, e.g., vanadium, is needed for refrigeration above about 500 mK. In this letter, we demonstrate both Al–Si and V–Si tunnel junctions with small R_A. We discuss the optimization of a cascade cooler with multiple refrigeration stages (Fig. 1(a)) and in particular, we evaluate how the finite cooling efficiency affects the complete thermal balance.

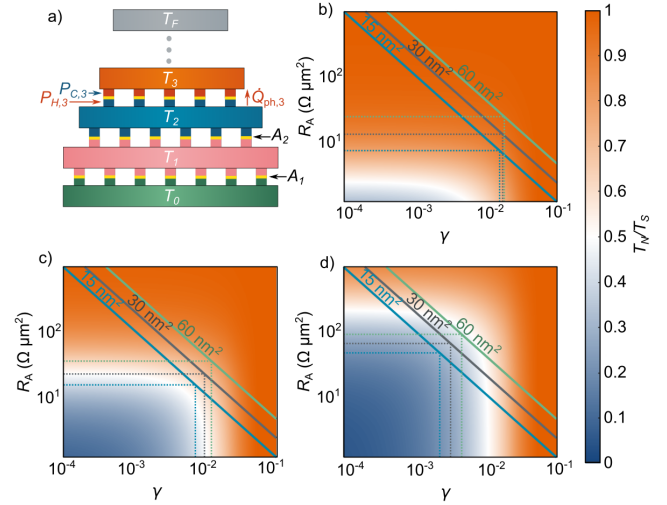The cooling power of NIS or Sm–S tunnel junction is lim-

FIG. 1. (a) Schematic picture of a cascaded refrigrerator with F stages. A macroscopic refrigerator provides the base temperature T_0, and each stage n has different total area A_n of tunnel junctions (yellow) and temperature T_n. The thermal balance of stage n is defined by the cooling power $P_{C,n}$, phonon heat leak $\dot{Q}_{\text{ph},n}$ from the previous stage $n-1$, and the heating power $P_{H,n+1}$ resulting from the refrigeration of the next stage $n+1$. (b-d) Optimisation between γ and R_A at $T_S = 0.8$ K with V–Si junctions. The three solid lines indicate the trade-off between R_A and γ for $A_{\text{eff}} = 15, 30$, and 60 nm^2 from left to right, respectively. The dotted lines indicate the optimal γ and R_A on each line. The only difference for panels (b-d) is the phonon heat conductance, which is 3900 W/m^{2}K^2, 390 W/m^{2}K^2, and 39 W/m^{2}K^2 for panels (b-d), respectively.

ited by the leakage resistance R_0 in the sub-gap regime, especially at temperatures well below the critical temperature of the superconductor $T \ll T_c$. The sub-gap leakage can originate from nonidealities of the superconductor or the tunnel junction, but the fundamental limit is defined by the Andreev reflection [15, 16]. According to theory for opaque NIS junctions [17], the sub-gap leakage parameter $\gamma = R_0/R_T$ due to Andreev reflection, is inversely proportional to the characteristic resistance $\gamma = A_{\text{ch}} R_K/(4 R_A)$. Here, A_{ch} is the area of one conduction channel, $R_K = h/e^2$ is the quantum resistance, e is the elementary charge and h is the Planck constant. We use an

effective channel area

$$A_{\text{eff}} = \frac{4\gamma R_A}{R_K} \qquad (1)$$

as a figure of merit for our tunnel junction, which describes the trade-off between γ and R_A. The observed channel areas of Andreev limited Al–AlO–Cu junctions have been of the order of 30 nm^2, which is about decade higher than theoretical estimates [17]. This has been accounted for slight inhomogeneities of the tunnel barrier, and exponentially dependent tunneling probabilities.

Figures 1(b–d) demonstrate the tradeoff between γ and R_A for relative cooling T_N/T_S with a V–Si junction at superconductor temperature $T_S = 0.8$ K and with superconducting energy gap $\Delta_V = 600$ μeV [18] ($T_c = 3.95$ K). We assume that the phonon heat current is $\dot{Q}_{\text{ph}} = g_{\text{ph}}A(T_S^4 - T_N^4)$. Figure 1(b) shows results obtained with the prefactor $g_{\text{ph}} = 3900$ W/m^{2}K^2 that is expected for the Kapitza interface [13]. Figures 1(c–d) demonstrate cases where the phonon heat conductance has been suppressed by factors 10 and 100, respectively. The more transparent junctions, i.e., lower R_A with cost of having higher γ, are favored when the phonon heat conductance is high. The suppression of the phonon heat conductance shifts the preference to higher R_A and related lower γ but overall Figs. 1(b-d) motivate the fabrication of tunnel junctions with $R_A < 100$ $\Omega\mu$m^2.

Figure 2(a) shows the voltage–current characteristics of Al–Si and an V–Si junctions fabricated with similar process than in Ref. [19] but with aim of increased junction transparency. The Al–Si junctions have 500 nm thick Al as superconductor but the V–Si junctions actually consists of a multilayer Al (25 nm) – V (150 nm) – Al (400 nm). The vanadium junctions require a thin layer of, e.g., Al, at the junction interface to allow high-quality junctions [10], but also the same layer and thickness of the V, can be used to tune the effective superconducting gap (Fig. 2(b)) between the gap of Al, $\Delta_{\text{Al}} = 200$ μeV, and the gap of pure V, $\Delta_V = 600$ μeV [18]. The thicker Al layer on top reliefs the multilayer film strain, but it also provides efficient means for quasiparticle diffusion. The Al–Si junction has the characteristic tunneling resistance of about $R_A \approx 48$ $\Omega\mu$m^2, which is a factor 10 improvement compared to the results of Ref.[13]. The sub-gap leakage parameter of the junction is $\gamma = 8 \times 10^{-3}$, which yields $A_{\text{eff}} = 62$ nm^2. The similar parameters for the V–Si junction are $R_A \approx 71$ $\Omega\mu$m^2, $\gamma = 6 \times 10^{-3}$, and $A_{\text{eff}} = 65$ nm^2. This is a significant improvement to previous results with S–Si junctions [13, 19]. Our results yield an encouraging upper limit of $A_{\text{ch}} \lesssim 60$ nm^2 for the strength of Andreev reflection in our Sm–S junctions, which is only factor 2 higher than the Andreev limit observed for Al–Cu junctions [17]. There is no reference value for A_{ch} in Sm–S junctions and we have not yet observed any indication that we would be at this fundamental limit.

The optimisation in Fig. 1 and in existing literature only optimises the cooling of a single stage without taking into account cooling efficiency, i.e., the ratio between cooling power one side of the refrigeration stage, P_C, and related heating the other, P_H. This approach is usually valid for the first stage of the cascade, if the macroscopic refrigerator provides the base
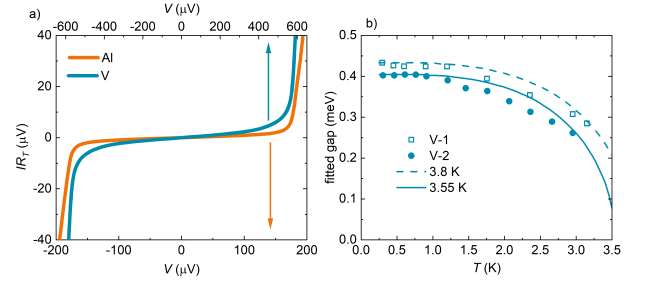

FIG. 2. (a) Current–voltage characteristics of Al–Si (orange) and V–Si (blue) junctions with low leakage. Both junctions were measured in series with a similar junction, but significantly larger area. This may have an effect on the observed superconducting gap, but not to the measurement of γ. (b) The superconducting energy gap of two V–Si junctions as a function temperature obtained from tunnelling rate fits to the IV(T)s (circles and squares). The lines are the best matching Bardeen-Cooper-Schrieffer theory superconducting energy gaps corresponding to critical temperatures of 3.55 K and 3.8 K.

temperature T_0 with large cooling power $P_0 \gg P_H$. However, cooling of stage n in Fig. 1(a) produces significant heating power for the subsequent stage $n-1$. Numerical optimization of the cascade refrigerator using the full heat balance is computationally demanding due to the large number of parameters that affect the system. Neither does that provide the physical insight of the system. Therefore, we developed an approximative method for optimising individual stages of the cascade.

The cooling power of an Sm–S or NIS junction is $P_C \approx 0.59\Delta^2/(eR_T) \times (k_bT_N/\Delta)^{3/2}$ [2]. The optimal cooling performance occurs roughly at a fixed ratio between T_N and T_c, since Δ limits cooling at high temperatures, and γ at low temperatures. Ideally, for any target cooling temperature T_N we use a superconductor with T_c that optimises the cooling power, i.e., T_N/T_c is fixed, which is possible, e.g., with the help of the proximity effect , see Fig. 2(b). Then we have $T_N \propto T_c \propto \Delta$, which yields $P_C \propto T_N^2 f(T_N/T_c) \propto T_N^2$ [13].

The cooling and heating powers of each stage n are proportional to the total area of tunnel junctions of the stage, i.e. $P_{C,n}, P_{H,n} \propto A_n$. The finite cooling efficiency means that $P_{H,n} \gg P_{C,n}$. If the heating of stage n is a dominant heat source of stage $n-1$, we have $P_{H,n} \approx P_{C,n-1} \approx (A_{n-1}/A_n) \times (T_{n-1}^2/T_n^2) \times P_{C,n}$, where T_n and T_{n-1} are the temperatures of stages n and $n-1$, respectively. We then obtain the ratio required for the areas of sequential stages

$$a_n = \frac{A_{n-1}}{A_n} \approx \frac{P_{H,n}T_n^2}{P_{C,n}T_{n-1}^2} \equiv \frac{P_H T_N^2}{P_C T_S^2}, \qquad (2)$$

The right hand side is written as a function of normal metal and superconductor temperatures of the stage under consideration, T_N, and T_S, respectively. The structure of the cascade refrigerator ensures that $T_N = T_n$, and $T_S = T_{n-1}$. The heat load caused by the cooling of the higher stages, $n = 2, \ldots, F$, requires the area ratio between the first and the last stages $A_1/A_F \equiv a = \prod_{n=2}^{F} a_n$.

An optimal cascade refrigerator has small a, since the goal is to have a compact device that provides the maximum cool-

ing power to the final stage. The constraint of this optimisation problem is the target cooling ratio T_1/T_F, where we assume that the first stage is optimized separately as in Fig. 1. To yield an approximative solution, we assume also that each stage $n = 2 \ldots F$ has the same a_n, i.e. $a = a_n^{F-1}$ and the same relative refrigeration performance T_S/T_N, i.e., $T_1/T_F = (T_S/T_N)^{F-1}$. Then we have $F - 1 = \lg(T_1/T_F)/\lg(T_S/T_N)$. This yields $a = O^{\lg(T_1/T_F)}$, where O is our optimization parameter

$$O \equiv \left(\frac{P_H T_N^2}{P_C T_S^2} \right)^{\frac{1}{\lg T_S - \lg T_N}}. \tag{3}$$

An optimal cascade refrigerator thus has refrigeration stages $n = 2 \ldots F$ that each have small O_n. It is important to note that O only depends of on the cooling and heating powers and the temperature difference of a single stage only. It allows us to optimize a single stage at a time, and to use it as a figure of merit for that stage. The optimization parameter O also does not explicitly depend on the experimental parameters such as γ, R_A, or g_{ph}, i.e., there may be several ways to obtain similar O. To gain intuitive insight to the magnitude of O, let us consider a realistic refrigeration objective, to cool from $T_1 = 1$ K to $T_F = 100$ mK. If all stages $n = 2, \ldots, F$ have the same $O = O_n$, the cascade then requires the total ratio of areas $A_1/A_F = O^{\lg(T_1/T_F)} = O$.

Below we will demonstrate the consequencies of O parameter optimization for specific cooler stages and cascades. We first demonstrate how O yields a different result than conventional cooler optimization. Then we study, how well Al–Si and V–Si junctions can perform as a higher $n \geq 2$ stage of a cascade. Finally, we consider the optimization of a specific refrigerator with 3 stages. In all examples below we vary γ and R_A using $A_{eff} = 15$ nm^2, which is in agreement with the targeted $\gamma = 10^{-3}$ and $R_A = 100$ $\Omega\,\mu$m^2 of Ref. [13].

Figure 3(a-b) show the relative cooling T_N/T_S and O, respectively, for Al–Si stage at 0.3 K. Both are presented as the function of γ and relative bias voltage $v = eV/\Delta$ where V is the absolute bias voltage. The minimum of O is obtained at smaller bias voltage than $v_{opt} = 1 - 0.66k_B T_N/\Delta$, which is the approximate voltage for the maximum cooling power [2]. It should be also noted that the optimisation of O yields smaller γ and higher R_A than the optimisation of T_N/T_S. This means that for cascaded stages, it is of advantage to sacrifice some of the cooling power in the lower temperature stages to suppress the heating of stages at higher temperature. For Figs. 3(c-d) we calculated O for Al-based ($\Delta = 200$ μeV) and V-based ($\Delta = 450$ μeV) refrigeration stages as a function T_S, g_{ph}, γ, and v. We show $O(T_S, g_{ph})$ where O has been optimized with respect to γ and v as shown in Fig. 3(b) for all combinations of T_S and g_{ph} separately. Regimes with $O \lesssim 10^2$ indicate roughly the operating regimes where Al- and V-based stages can be operated as a higher stage $n \geq 2$ of a cascade. The highest g_{ph} in Figs. 3(c-d) is the expected $g_{ph} = 3900$ W/m^{2}K^2 for a Kapitza interface. This indicates that an improvement of the phonon thermal resistance is important when the Al–Si junctions are used in a cascade, even though the Kapitza interface can be sufficient for a single Al–Si stage [13]. Aluminium
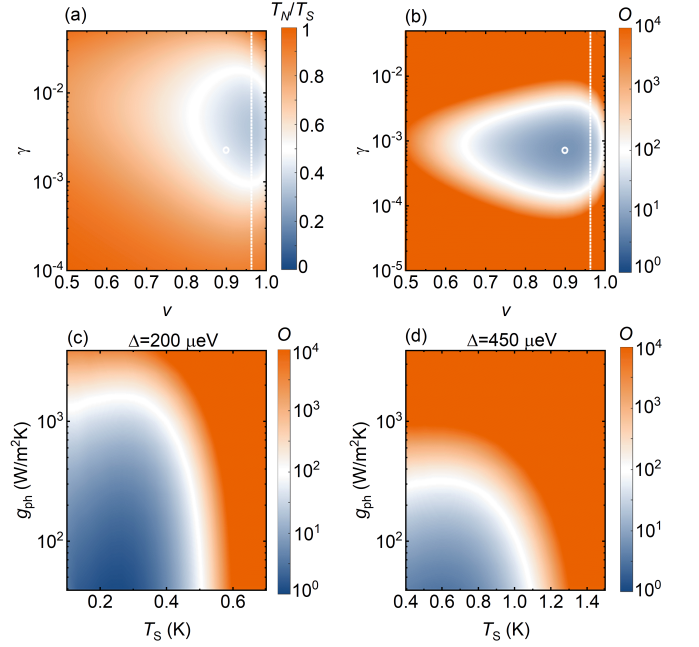

FIG. 3.   (a-b) Al–Si refrigerator stage at $T_S = 0.3$ K with $g_{ph} = 390$ W/m^{2}K^2, and $A_{eff} = 15$ nm^2. (a) Relative cooling T_N/T_S as function of γ and $v = eV/\Delta$. (b) Optimisation parameter O as a function of v and γ. The minimum position of O is denoted by white circle in both (a) and (b). The expected optimum bias voltage v_{opt} for T_N of minimum O is shown by the dotted white line. (c-d) The optimal O with respect to v and γ for Al-based ($\Delta = 200$ μeV) and V-based ($\Delta = 450$ μeV) refrigeration stages, respectively.

can be used for refrigeration below about 500 mK, but above that, a superconductor with higher Δ is needed. However, a superconductor with higher Δ requires even lower g_{ph}.

Figures 4(a-d) show the parameters obtained from the optimization of Figs. 3(c-d) as a function of T_S for three values of g_{ph}. These results demonstrate that the optimal γ varies significantly as a function of temperature and phonon heat conductance, and that high temperature and phonon heat conductance yield high optimal γ, which is expected since then low R_A maximizes cooling power. Optimization parameter O gets very high values for non-optimal refrigeration stages, which stringent requirements for a practical cascade refrigerator. However, Fig. 4(c) shows that Al and V can be used in a cascade below about 500 mK and 1 K, respectively

Finally, we compare temperature optimizations based on optimizing parameter O and on the full heat balance. Experimentally, a desired starting temperature would be $T_0 > 1.2$ K, which is achievable with refrigerators based on ^{4}He. This motivates to consider a refrigerator that consists of 3 stages with $\Delta_1 = 600$ μeV, $\Delta_2 = 450$ μeV, and $\Delta_3 = 200$ μeV, where both Δ_1 and Δ_2 can be achieved with V–Si junctions. The first stage is optimised as in Fig. 1, and the other by minimizing O_2 and O_3. The black symbols and lines of Fig. 4(d) illustrate the refrigeration performance of stages 2 and 3, when the first stage yields temperature $T_1 = 0.8$ K. The very low
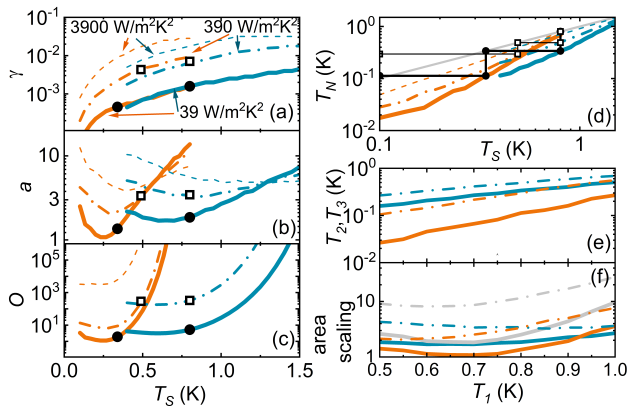
FIG. 4. Results from the optimization of O with respect to v and γ for Al-based ($\Delta = 200$ μeV, orange) and V-based ($\Delta = 450$ μeV, blue) refrigeration stages. Data with $g_{\mathrm{ph}} = 3900$ W/m^{2}K^2, 390 W/m^{2}K^2, and 39 W/m^{2}K^2 are shown with dashed, dash-dotted, and solid lines, respectively. (a) Optimal γ as a function T_S. (b) The required area scaling a_n as a function of T_S. (c) O as a function of T_S. Vanadium stage with $g_{\mathrm{ph}} = 3900$ W/m^{2}K^2 has $O > 10^6$, which is beyond the figure scale. (d) T_N as a function of T_S. The grey line shows the threshold for cooling, i.e., $T_N = T_S$. The black lines and symbols illustrate refrigeration performance in the case where a first stage cooler provides $T_1 = 0.8$ K, the second stage is based on V ($\Delta = 450$ μeV, blue), and third stage on Al ($\Delta = 200$ μeV, orange). The cases $g_{\mathrm{ph}} = 390$ W/m^{2}K^2 and 39 W/m^{2}K^2 are denoted with open squares and closed circles, respectively. (e) Refrigeration performance (T_2 and T_3 are blue and orange, respectively) as a function of T_1 of a cascade with V-based ($\Delta = 450$ μeV) second stage and Al-based third stage. (f) Parameters a_2, a_3, and $a = a_2 a_3$ (blue, orange, and grey lines, respectively) as a function of T_1 for the cascade of (e).

phonon heat conductance $g_{\mathrm{ph}} \approx 39$ W/m^{2}K^2 allows to reach $T_3 = 100$ mK. Figure 4(e) shows T_2 and T_3 as a function of T_1. Figure 4(f) shows the required area scalings a_2, a_3, and $a = a_2 a_3$ for the refrigeration results of Fig. 4(e). Our conclusion from Figs. 4(e-f) is that it is very demanding to build a cascade refrigerator that cools a sample from above 1 K to below 100 mK, but if such a device is built, the area scaling can be as low as $a \sim 10$, which enables a very compact device. Table I shows a comparison between results obtained from the O parameter approximative optimization and the full heat balance for the 3-stage refrigerator. There is a relatively

good agreement between the approximation and the full heat balance, if the area scalings are multiplied with a small factor of 2...3.

To conclude, we have developed an optimization protocol for cascaded electronic refrigerators based on NIS or Sm–S tunnel junctions, which takes into account the heating generated in the cascaded device. We use it to show the required criteria using a cascade of Al–Si and V–Si tunnel junctions for refrigeration from above 1 K down to about 100 mK. Our analysis shows that energy efficient refrigeration stages are required to mitigate the heating of cascaded refrigeration stages and demonstrates the importance of phonon engineering and optimization of tunnel junctions. Furthermore, we have ex-

TABLE I. Example of thermal balance with $A_{\mathrm{ch}} = 15$ nm^2. Here, T_{est} are temperatures estimated from the optimisation of single stages using parameter O, and $T_{\mathrm{m=k}}$ are the temperatures obtained from the thermal balance of the whole cascade, where m is an extra multiplier for the areas. For $m = 1$ the areas used for the thermal balance are exactly a_n. For $m = k$, the areas the second and the first stage is $k \times a_2$, and $k^2 \times a_1$, respectively. Values for g_{ph}, γ and v are obtained from optimization of O. Same parameters are used in the simulations of the full model.

			$T_0 = 1.2$ K					
n	T_{est} (K)	$T_{\mathrm{m=3}}$ (K)	$T_{\mathrm{m=1}}$ (K)	A_n/A_3	g_{ph} (W/m^{2}K^2)	γ (10^{-3})	v	O_n
1	0.70	0.72	0.82	4.5	160	10	v_{opt}	
2	0.33	0.37	0.54	1.7	160	3.2	0.90	21
3	0.13	0.15	0.36	1	160	1.3	0.90	3.5

perimentally demonstrated transparent Al–Si and V–Si tunnel junctions, which set an upper limit for $A_{\mathrm{ch}} \lesssim 60$ nm^2 for the channel area of Andreev reflection in both types of junctions, which is already close results on NIS junctions [17].

[1] J. M. Martinis and M. Nahum, Physical Review B **48**, 18316 (1993).

[2] M. M. Leivo, J. P. Pekola, and A. D. V, Applied Physics Letters **68**, 1996 (1996).

[3] A. M. Savin, M. Prunnila, P. P. Kivinen, J. P. Pekola, J. Ahopelto, and A. J. Manninen, Applied Physics Letters **79**, 1471 (2001), https://doi.org/10.1063/1.1399313.

[4] F. Giazotto, T. T. Heikkilä, A. Luukanen, A. M. Savin, and J. P. Pekola, Rev. Mod. Phys. **78**, 217 (2006).

[5] P. J. Lowell, G. C. O'Neil, J. M. Underwood, and J. N. Ullom, Applied Physics Letters **102**, 082601 (2013),

https://doi.org/10.1063/1.4793515.

[6] N. A. Miller, G. C. O'Neil, J. A. Beall, G. C. Hilton, K. D. Irwin, D. R. Schmidt, L. R. Vale, and J. N. Ullom, Applied Physics Letters **92**, 163501 (2008), https://doi.org/10.1063/1.2913160.

[7] A. M. Clark, N. A. Miller, A. Williams, S. T. Ruggiero, G. C. Hilton, L. R. Vale, J. A. Beall, K. D. Irwin, and J. N. Ullom, Applied Physics Letters **86**, 173508 (2005), https://doi.org/10.1063/1.1914966.

[8] H. Q. Nguyen, M. Meschke, and J. P. Pekola, Applied Physics Letters **106**, 012601 (2015), https://doi.org/10.1063/1.4905440.

[9] P. J. Koppinen and I. J. Maasilta, Phys. Rev. Lett. **102**, 165502 (2009).

[10] O. Quaranta, P. Spathis, F. Beltram, and F. Giazotto, Applied Physics Letters **98**, 032501 (2011), https://doi.org/10.1063/1.3544058.

[11] H. Q. Nguyen, J. T. Peltonen, M. Meschke, and J. P. Pekola, Phys. Rev. Applied **6**, 054011 (2016).

[12] M. Camarasa-Gómez, A. Di Marco, F. W. J. Hekking, C. B. Winkelmann, H. Courtois, and F. Giazotto, Applied Physics Letters **104**, 192601 (2014), https://doi.org/10.1063/1.4876478.

[13] E. Mykkänen, J. S. Lehtinen, L. Grönberg, A. Shchepetov, A. V. Timofeev, D. Gunnarsson, A. Kemppinen, A. J. Manninen, and M. Prunnila, Science Advances **6** (2020), 10.1126/sciadv.aax9191, https://advances.sciencemag.org/content/6/15/eaax9191.full.pdf.

[14] E. T. Swartz and R. O. Pohl, Applied Physics Letters **51**, 2200 (1987), https://doi.org/10.1063/1.98939.

[15] A. F. Andreev, Zh. Eksp. Teor. Fiz. , 1823 (1964), [Sov.Phys. JETP19, 1228 (1964)].

[16] S. Rajauria, P. Gandit, T. Fournier, F. W. J. Hekking, B. Pannetier, and H. Courtois, Phys. Rev. Lett. **100**, 207002 (2008).

[17] V. F. Maisi, O.-P. Saira, Y. A. Pashkin, J. S. Tsai, D. V. Averin, and J. P. Pekola, Phys. Rev. Lett. **106**, 217003 (2011).

[18] C. P. García and F. Giazotto, Applied Physics Letters **94**, 132508 (2009).

[19] D. Gunnarsson, J. S. Richardson-Bullock, M. J. Prest, H. Q. Nguyen, A. V. Timofeev, V. A. Shah, T. E. Whall, E. H. C. Parker, D. R. Leadley, M. Myronov, and M. Prunnila, Scientific Reports **5** (2015), 10.1038/srep17398.